Discrete Least Square Dual Solutions of Cauchy-Riemann Equations

Hiroaki Nishikawa and Philip L. Roe

Summer, 1997

Abstract

This paper concerns the choice of the norm for Cauchy-Riemann equations in the discrete least square formulation. Two different types of norms are studied in detail. It is shown that the two norms approximate solutions in both physical and hodograph planes in two different ways. Also one way to determine the safety factor is presented. It greatly improved the convergence of the method. Finally some numerical results are presented.

1 Introduction

The strategy of finding an approximate solution is described in [1]. Here only a brief review is given. Let us divide the domain of interest into a set $\{T_p\}$ of triangular elements where the subscript p denotes the physical plane on which a governing equation is expressed in a usual sense. All the quantities are stored at vertices and vary linearly within the element. Then first order differential operators are constant in each element, implying constant residuals of first order differential equations. Such constant residuals are also called fluctuations Φ_T. Suppose there are n fluctuations in each element where n is the number of equations to be approximated, then we attempt to minimize

$$\mathcal{F} = \sum_{T\in\{T_p\}} F_T = \frac{1}{2}\sum_{T\in\{T_p\}} \Phi_T^t Q_T \Phi_T \tag{1}$$

where Q_T is an $n \times n$ positive definite symmetric matrix. The matrix Q_T gives weights to each fluctuation within each element. It it this matrix that characterizes a numerical scheme derived from the least square method. It is not surprising that two different choices of Q_T produce completely different least square solutions. The derivative of the norm above with respect to a particular nodal value u_j (solution or coordinate) is the sum of the contributions from the elements that share that vertex,

$$\frac{\partial \mathcal{F}}{\partial u_j} = \sum_{T\in\{T_{p,j}\}} \Phi_T^t \left(Q_T \frac{\Phi_T}{\partial u_j} + \frac{1}{2}\frac{Q_T}{\partial u_j}\Phi_T \right) \quad . \tag{2}$$

At a minimum this quantity vanishes. In order to search for such a minimum we follow a path of steepest descent. Thus

$$\delta u_j = -c\frac{\partial \mathcal{F}}{\partial u_j} = -c \sum_{T\in\{T_{p,j}\}} \Phi_T^t \left(Q_T \frac{\Phi_T}{\partial u_j} + \frac{1}{2}\frac{Q_T}{\partial u_j}\Phi_T \right) \tag{3}$$

where c is a small constant. With any choice of Q_T that is independent of the solution we have a quadratic norm, thus guarranteeing a unique minimum. However once Q_T involves the solution (the norm becomes nonquadratic.), there is not always a unique minimum. It is again the choice of Q_T that holds the key to the success of the method.

Our aim is to apply the method to elliptic problems with singularities and to investigate whetherthe solution is improved by grid movement. This can be done, we hope, by solving hodograph equations (governing equations with independent and dependent variables exchanged). Although it is possible to achieve higher resolution by refining a grid, we attempt to achive this as much as we can with a fixed amount of resource. Also we do not monitor intermediate solutions to make corrections to a grid, instead we believe that the key to an optimal grid is hidden in governing equations. The future application includes clearly the reasonable resolution of boundary layers.

In this paper, we study the Cauchy-Riemann equations that appear in two dimensional incompressible potential flow. The equations are simple and easily transformed into the hodograph equations. This simplicity allows us to learn much from it. In the next section, we define the hodograph transformation. And then we present a way to integrate the equations and show that residuals are identical in physical and hodograph planes. In

the following section, we study two different norms in detail. We shall see how different these norms are. In section 5, the implementation and the choice of the safety factor c is discussed. We give some numerical results in section 6.

2 Governing equations

In two dimension an incompressible and irrotational flow is governed by

$$\frac{\partial \phi}{\partial x} - \frac{\partial \psi}{\partial y} = 0 \tag{4}$$

$$\frac{\partial \phi}{\partial y} + \frac{\partial \psi}{\partial x} = 0 \tag{5}$$

where ϕ and ψ are a velocity potential and a stream function respectively. It is possible to exchange the independent and dependent variables to get governing equations for x and y in $\phi - \psi$ plane, which is known as hodograph transformation. Let us define the transformation as follows.

$$\partial_\phi x = \partial_y \psi / j, \;\; \partial_\psi x = -\partial_y \phi / j, \;\; \partial_\phi y = -\partial_x \psi / j, \;\; \partial_\psi y = \partial_x \phi / j \tag{6}$$

where

$$j = \partial_x \phi \partial_y \psi - \partial_y \phi \partial_x \psi = (\partial_\psi y \partial_\phi x - \partial_\psi x \partial_\phi y)^{-1}. \tag{7}$$

We then have another set of Cauchy-Riemann equations.

$$\frac{\partial y}{\partial \psi} - \frac{\partial x}{\partial \phi} = 0 \tag{8}$$

$$-\frac{\partial y}{\partial \phi} - \frac{\partial x}{\partial \psi} = 0 \tag{9}$$

Note that the Jacobian defined in this way is always positive (Substitute (4) and (5) into (7) to see this), which in turn implies that the transformation has been defined between (x, y) plane and (ϕ, ψ) plane with the same orientations. We shall see in the next section that the discretized versions of the two systems are identical.

3 Discretization

The residuals are in general obtained by integrating the governing equations over an element T, invoking Green's theorem. It is however also possible to discretize the equations in the following way. In our representation of solutions, we have the interpolation formula within an element for ϕ and ψ given by

$$\phi = \sum_{i \in j_{T_p}} \phi_i N_i(x, y), \;\; \psi = \sum_{i \in j_{T_p}} \psi_i N_i(x, y) \tag{10}$$

where

$$N_i(x, y) = \frac{a_i + b_i x + c_i y}{2 S_p} \tag{11}$$

$$a_i = x_k y_l - y_k x_l \tag{12}$$
$$b_i = \Delta y_i \tag{13}$$
$$c_i = -\Delta x_i \tag{14}$$

and S_p is the area of the element given by

$$S_p = \frac{1}{2} \sum_{i \in j_{T_p}} x_i \Delta y_i = -\frac{1}{2} \sum_{i \in j_{T_p}} y_i \Delta x_i \tag{15}$$

where $\Delta\{\}_i$ denotes a difference taken counterclockwise along the side opposite to j and the subscripts k and l take 1, 2 and 3, and are permuted cyclically for i. Simple differentiation of the formula yields

$$\frac{\partial \phi}{\partial x} = \frac{1}{2S_p} \sum_{i \in j_{T_p}} \phi_i \Delta y_i, \quad \frac{\partial \phi}{\partial y} = -\frac{1}{2S_p} \sum_{i \in j_{T_p}} \phi_i \Delta x_i \tag{16}$$
$$\frac{\partial \psi}{\partial x} = \frac{1}{2S_p} \sum_{i \in j_{T_p}} \psi_i \Delta y_i, \quad \frac{\partial \psi}{\partial y} = -\frac{1}{2S_p} \sum_{i \in j_{T_p}} \psi_i \Delta x_i \tag{17}$$

which are all constants in an element. Thus the integration of the derivatives over the element becomes the multiplication of the derivatives and the area. With the use of these equations, the integration of the first order PDE becomes a simple task. We thus have the following residuals of the Cauchy-Riemann equations in the physical plane.

$$U_T = \frac{1}{2} \sum_{i \in j_{T_p}} \phi_i \Delta y_i + \frac{1}{2} \sum_{i \in j_{T_p}} \psi_i \Delta x_i \tag{18}$$
$$V_T = \frac{1}{2} \sum_{i \in j_{T_p}} \psi_i \Delta y_i - \frac{1}{2} \sum_{i \in j_{T_p}} \phi_i \Delta x_i \tag{19}$$

Suppose that we have a set of triangles in the hodograph plane, a set $\{T_h\}$ and that there is a one-to-one correspondence between $\{T_h\}$ and $\{T_p\}$. And remember that the orientations in the two planes are the same due to the positive Jacobian, thus allowing the all of the above formulas to be valid in the hodograph plane as well. Then in the same way, but in (ϕ, ψ) plane, we obtain

$$\frac{\partial x}{\partial \phi} = \frac{1}{2S_h} \sum_{i \in j_{T_h}} x_i \Delta \psi_i, \quad \frac{\partial x}{\partial \psi} = -\frac{1}{2S_h} \sum_{i \in j_{T_h}} x_i \Delta \phi_i \tag{20}$$
$$\frac{\partial y}{\partial \phi} = \frac{1}{2S_h} \sum_{i \in j_{T_h}} y_i \Delta \psi_i, \quad \frac{\partial y}{\partial \psi} = -\frac{1}{2S_h} \sum_{i \in j_{T_h}} y_i \Delta \phi_i \tag{21}$$

Then simple integration over an element T_h yields the residuals that take exactly the same form as those in the physical plane, i.e. equations (16) and (17). This particular formulation is equally applicable to the physical or hodograph representations.

4 Norms and Gradients

4.1 Norms

In this section we discuss the choice of the norm that we attempt to minimize. Naturally the norm can be defined as some positive function of the residuals. Here we discuss two norms. Let us first consider the following norm.

$$\mathcal{F}_s = \sum_{T\in\{T_p\}} F_{s_T} = \sum_{T\in\{T_p\}} \frac{1}{2}\left[{U_T}^2 + {V_T}^2\right] \tag{22}$$

Note we have chosen the matrix Q_T as an identity matrix. It is easy to show that this norm can be rewritten as

$$\mathcal{F}_s = \sum_{T\in\{T_p\}} \frac{S_T}{2}\iint_T \nabla\phi\cdot\nabla\phi\, dxdy + \sum_{T\in\{T_p\}} \frac{S_T}{2}\iint_T \nabla\psi\cdot\nabla\psi\, dxdy - \sum_{T\in\{T_p\}} S_T S_T(\phi,\psi) \tag{23}$$

where $S_T(\phi,\psi)$ is the area of the element in (ϕ,ψ) plane corresponding to element $T \in \{T_p\}$. Also in view of the hodograph plane, this can be rewritten as

$$\mathcal{F}_s = \sum_{T\in\{T_h\}} \frac{S_T}{2}\iint_T \nabla x\cdot\nabla x\, d\phi d\psi + \sum_{T\in\{T_h\}} \frac{S_T}{2}\iint_T \nabla y\cdot\nabla y\, d\phi d\psi - \sum_{T\in\{T_h\}} S_T S_T(x,y) \tag{24}$$

where $S_T(x,y)$ is the area of the element in (x,y) plane corresponding to element $T \in \{T_h\}$. Therefore, as it should, this norm takes the same form in both physical and hodograph planes. We refer this type of norm as symmetric. We will compare this with a weighted Least-squares formulation using the element areas in the physical plane as weights. That is to say,

$$\mathcal{F}_a = \sum_{T\in\{T_p\}} F_{a_T} = \sum_{T\in\{T_p\}} \frac{1}{2S_T}\left[{U_T}^2 + {V_T}^2\right] \quad . \tag{25}$$

We have chosen the matrix Q_T as an identity matrix times $\frac{1}{S_T}$. As in the previous case, this also can be rewritten as

$$\mathcal{F}_a = \sum_{T\in\{T_p\}} \frac{1}{2}\iint_T \nabla\,\phi\cdot\nabla\phi\, dx\, dy + \sum_{T\in\{T_p\}} \frac{1}{2}\iint_T \nabla\,\psi\cdot\nabla\psi\, dx\, dy - \sum_{T\in\{T_h\}} S_T \tag{26}$$

$$\mathcal{F}_a = \sum_{T\in\{T_h\}} \frac{J_T}{2}\iint_T \nabla\, x\cdot\nabla x\, d\phi\, d\psi + \sum_{T\in\{T_h\}} \frac{J_T}{2}\iint_T \nabla\, y\cdot\nabla y\, d\phi\, d\psi - \sum_{T\in\{T_h\}} S_T \tag{27}$$

where J_T is the discrete version of the Jacobian in element T. Note that asymmetry arises due to the presence of $\frac{1}{S_T}$. We call this type of norm an asymmetric norm. Note that the last terms are simply the areas of the entire domains in physical and hodograph planes respectively. Hence these terms do not involve any interior variables (area is determined by its boundary values), thus excluding themselves from the minimization problem inside the domain. In effect, these terms on the boundary play their roles as implementing the natural boundary conditions. The same holds true for the symmetric norm, except that on an unstructured grid they do involve the interior variables and thus participating the minimization problem.

From the two different norms defined above, we first observe the following fact. *The symmetric norm is always positive while the asymmetric one can be negative if the area of the triangle becomes negative in the physical plane.* This implies that the minimization problem turns to the maximization for the asymmetric norm. This is a trouble. Negative area in the hodograph plane, on the other hand, does not cause any trouble because of J_T in the equation (27), which has the same sign as $S(\phi, \psi)$ and thus keeps the norm positive. Therefore it is expected that no sooner does mesh tangling occur than solutions blow up if the asymmetric norm is used. Conversely for the symmetric norm, mesh tangling can never be detected during the minimization.

Secondly, *whereas the symmetric norm provides two linear problems in both physical and hodograph planes, the asymmetric norm create a linear problem in physical plane and a nonlinear problem in hodograph plane.* In practice, we perform a minimization alternately in physical and hodograph planes [5]. The norms we defined are indeed nonlinear provided (x, y, ϕ, ψ) are treated as a set of variables. However we can work on linear problems by treating only two variables per iteration. This is a great rescue. But this does not apply to the asymmetric norm. The problem becomes nonlinear in hodograph plane even if the alternating strategy is employed. The convergence is expected to be slow for the asymmetric norm.

Thirdly, *for the asymmetric norm, mesh adaptation is driven by Jacobians and carried out in the hodograph plane while the standard method finds solutions for a given grid at each step. On the other hand, the symmetric norm yields exactly the same type of scheme in both planes, in which both mesh adaptation and its counter mechanism are incorporated.* In equation (26), it is clearly seen that minimizing the first two terms is equivalent to the standard finite element method applied to the two Laplace equations for ϕ and ψ in the physical plane. Then similar terms in (27) can be interpreted as the standard method with Jacobians as weights. Therefore it is reasonable to think that large Jacobians drive mesh adaptation in x-y plane, by giving a large weight to the norm in the element relative to which the corresponding element area in ϕ-ψ plane is large. In the similar way, minimizing the first two terms in (23) and (24) can also be considered as the standard methods with element areas in each plane as weights. Hence mesh adaptation in x-y plane is driven by a large element area in ϕ-ψ plane, and inversely mesh adaptation in ϕ-ψ plane is driven by a large element area in x-y plane. The last terms in (23) and (24), on the other hand, attempt to limit the adaptations. Note that these terms have negative signs in front and remember again that areas in both planes are positive. This means that we actually maximize the magnitudes of these terms, i.e. element areas, by minimizing the symmetric norm. These terms then can be considered as limiting an excessive node movement caused by the first two terms. This sort of mechanism is not clearly seen in the asymmetric norm. The discussion on this is given in the next section.

4.2 Gradients

We now extend our investigation to the gradients. From equations (22) and (25), the gradients for the symmetric and asymmetric norms with respect to the solutions $\mathbf{U}_j =$

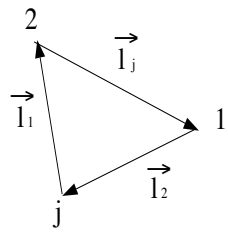

Figure 1: A triangle with side vectors.

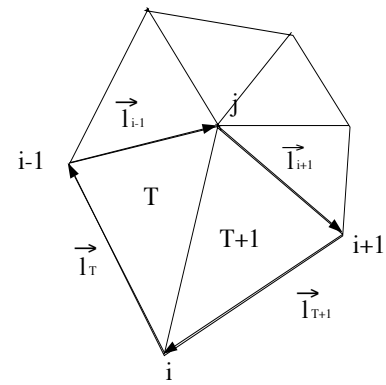

Figure 2: A group of triangles, $\{T_j\}$.

$(\phi_j, \psi_j, x_j, y_j)$ are obtained as

$$\frac{\partial \mathcal{F}_s}{\partial \mathbf{U}_j} = \sum_{T \in \{T_{p_j}\}} \begin{bmatrix} \frac{1}{2}\Delta y_T U_T - \frac{1}{2}\Delta x_T V_T \\ \frac{1}{2}\Delta x_T U_T + \frac{1}{2}\Delta y_T V_T \\ -\frac{1}{2}\Delta \psi_T U_T + \frac{1}{2}\Delta \phi_T V_T \\ -\frac{1}{2}\Delta \phi_T U_T - \frac{1}{2}\Delta \psi_T V_T \end{bmatrix} \tag{28}$$

$$\frac{\partial \mathcal{F}_a}{\partial \mathbf{U}_j} = \sum_{T \in \{T_{p_j}\}} \frac{1}{S_T} \begin{bmatrix} \frac{1}{2}\Delta y_T U_T - \frac{1}{2}\Delta x_T V_T \\ \frac{1}{2}\Delta x_T U_T + \frac{1}{2}\Delta y_T V_T \\ -\frac{1}{2}\Delta \psi_T U_T + \frac{1}{2}\Delta \phi_T V_T - \frac{1}{4S_T}\left({U_T}^2 + {V_T}^2\right)\Delta y_T \\ -\frac{1}{2}\Delta \phi_T U_T - \frac{1}{2}\Delta \psi_T V_T + \frac{1}{4S_T}\left({U_T}^2 + {V_T}^2\right)\Delta x_T \end{bmatrix} \tag{29}$$

respectively, where $\Delta\{\}_T$ denotes a difference taken counterclockwise along the side of triangle $T \in T_j$. Let us first consider physical plane. Expand the first component of (28), which drives the corrections to ϕ, as

$$\frac{\partial \mathcal{F}_s}{\partial \phi_j} = \frac{1}{2}\sum_{T \in \{T_{p_j}\}} \Delta y_T U_T - \frac{1}{2}\sum_{T \in \{T_{p_j}\}} \Delta x_T V_T \tag{30}$$

$$= \frac{1}{4}\sum_{T \in \{T_{p_j}\}} \Delta y_T \sum_{i \in j_T} \phi_i \Delta y_i + \frac{1}{4}\sum_{T \in \{T_{p_j}\}} \Delta x_T \sum_{i \in j_T} \phi_i \Delta x_i \tag{31}$$

$$+\frac{1}{4}\sum_{T \in \{T_{p_j}\}} \Delta y_T \sum_{i \in j_T} \psi_i \Delta x_i - \frac{1}{4}\sum_{T \in \{T_{p_j}\}} \Delta x_T \sum_{i \in j_T} \psi_i \Delta y_i \quad .$$

By using the following formulas,

$$\Delta y_j \sum_{i \in j_T} a_i \Delta y_i + \Delta x_j \sum_{i \in j_T} a_i \Delta x_i = \vec{l}_j \cdot \vec{l}_j a_j + \vec{l}_1 \cdot \vec{l}_j a_1 + \vec{l}_2 \cdot \vec{l}_j a_2 \tag{32}$$

$$\Delta y_j \sum_{i \in j_T} a_i \Delta x_i - \Delta x_j \sum_{i \in j_T} a_i \Delta y_i = 2S_T \Delta a_j \tag{33}$$

we obtain

$$\frac{\partial \mathcal{F}_s}{\partial \phi_j} = \left(\frac{1}{4}\sum_{T \in T_{p_j}} \vec{l}_T \cdot \vec{l}_T\right)\phi_j + \frac{1}{4}\sum_{i \in i_j}\left(\vec{l}_{i-1} \cdot \vec{l}_T + \vec{l}_{i+1} \cdot \vec{l}_{T+1}\right)\phi_i - \frac{1}{2}\sum_{T \in T_{p_j}} S_T \Delta \psi_T \quad . \tag{34}$$

This form can also be obtained directly from equation (23). Similarly for the second component, we have

$$\frac{\partial \mathcal{F}_s}{\partial \psi_j} = \left(\frac{1}{4} \sum_{T \in T_{p_j}} \vec{l}_T \cdot \vec{l}_T \right) \psi_j + \frac{1}{4} \sum_{i \in i_j} \left(\vec{l}_{i-1} \cdot \vec{l}_T + \vec{l}_{i+1} \cdot \vec{l}_{T+1} \right) \psi_i + \frac{1}{2} \sum_{T \in T_{p_j}} S_T \Delta \phi_T \quad . \tag{35}$$

The last terms will vanish for interior node j if for example all the triangles surrounding j have the same areas or ϕ is uniform along the sides opposite to j. There are still other circumstances, i.e. give all $\Delta\phi_T$, and all S_T except one, which can be solved for. Similarly for the asymmetric norm we obtain

$$\frac{\partial \mathcal{F}_a}{\partial \phi_j} = \left(\frac{1}{4} \sum_{T \in T_{p_j}} \frac{\vec{l}_T \cdot \vec{l}_T}{S_T} \right) \phi_j + \frac{1}{4} \sum_{i \in i_j} \left(\frac{\vec{l}_{i-1} \cdot \vec{l}_T}{S_T} + \frac{\vec{l}_{i+1} \cdot \vec{l}_{T+1}}{S_{T+1}} \right) \phi_i - \frac{1}{2} \sum_{T \in T_{p_j}} \Delta \psi_T \tag{36}$$

$$\frac{\partial \mathcal{F}_a}{\partial \psi_j} = \left(\frac{1}{4} \sum_{T \in T_{p_j}} \frac{\vec{l}_T \cdot \vec{l}_T}{S_T} \right) \psi_j + \frac{1}{4} \sum_{i \in i_j} \left(\frac{\vec{l}_{i-1} \cdot \vec{l}_T}{S_T} + \frac{\vec{l}_{i+1} \cdot \vec{l}_{T+1}}{S_{T+1}} \right) \psi_i + \frac{1}{2} \sum_{T \in T_{p_j}} \Delta \phi_T, \tag{37}$$

Evidently the last terms in the above expressions always identically vanish for interior nodes. Therefore the decoupling of ϕ and ψ occurs inside the domain. As mentioned in the previous section, the discretization is identical to the standard finite-element method. On the boundary, however, the last terms do not vanish. These are reduced to the difference of the two values adjacent to j along the boundary. This is irrelevant to updating ψ since we usually give the boundary condition for ψ everywhere on the boundary. However the boundary condition for ϕ is not given everywhere because ϕ can be determined up to an arbitrary additive constant. Therefore we update ϕ on the boundary, and thus the last terms are involved in the update of ϕ. It can be shown for a structured grid that each gradient is in fact the second order discretization of one of the Cauchy-Riemann equations that contains the derivetive of ψ along the boundary. Therefore the method automatically implement the appropriate natural boundary condition for ϕ.

Consider the first two terms in (34) and (35). These are slightly different from the standard method (Eqs. (36) and (37)) by a factor of S_T. On a structured grid, these two schemes are identical to each other. However they behave differently on an unstructured grid or once a grid starts to deform. The key to see this is the coefficients of the values at i in the second terms, which are the weights given to the values at the nodes connected with j. It can be shown that the standard method gives large weights to the values associated with small triangles in x-y plane. When viewed in the hodograph plane, this means that the changes to ϕ and ψ are such that the node j moves toward the triangles whose images in (x, y) have small areas. On the other hand, as for the symmetric norm, large weights are given to ϕ_i and ψ_i which are associated with large trisngles in x-y plane.

Also seen from the above results is the fact that we can solve a local problem exactly, i.e. the gradients can be made to be zero locally. Successive application of this is, in fact, a strategy similar to Gauss-Seidel method. Yet we can do better than this by applying the relaxation procedure, i.e. Succesive Over Relaxation(SOR) method. The use of equations (36) and (37) actually makes our scheme identical to SOR for the two Laplace equations for ϕ and ψ. However this is not true in general for the symmetric norm. This is because

the last terms will be involved in the scheme on unstructured grids, thus preventing the decoupling of the variables.

Now consider the gradients for x and y,

$$\frac{\partial \mathcal{F}_s}{\partial x_j} = \left(\frac{1}{4} \sum_{T \in \{T_{h_j}\}} \vec{l}_T \cdot \vec{l}_T \right) x_j + \frac{1}{4} \sum_{i \in i_j} \left(\vec{l}_{i-1} \cdot \vec{l}_T + \vec{l}_{i+1} \cdot \vec{l}_{T+1} \right) x_i - \frac{1}{2} \sum_{T \in \{T_{h_j}\}} S_T \Delta y_T \quad (38)$$

$$\frac{\partial \mathcal{F}_s}{\partial y_j} = \left(\frac{1}{4} \sum_{T \in \{T_{h_j}\}} \vec{l}_T \cdot \vec{l}_T \right) y_j + \frac{1}{4} \sum_{i \in i_j} \left(\vec{l}_{i-1} \cdot \vec{l}_T + \vec{l}_{i+1} \cdot \vec{l}_{T+1} \right) y_i + \frac{1}{2} \sum_{T \in \{T_{h_j}\}} S_T \Delta x_T \quad (39)$$

and for the asymmetric norm

$$\begin{aligned} \frac{\partial \mathcal{F}_a}{\partial x_j} &= \left(\frac{1}{4} \sum_{T \in \{T_{h_j}\}} J_T \frac{\vec{l}_T \cdot \vec{l}_T}{S_T} \right) x_j + \frac{1}{4} \sum_{i \in i_j} \left(J_T \frac{\vec{l}_{i-1} \cdot \vec{l}_T}{S_T} + J_{T+1} \frac{\vec{l}_{i+1} \cdot \vec{l}_{T+1}}{S_{T+1}} \right) x_i \quad (40) \\ &\quad - \frac{1}{16} \sum_{T \in \{T_{p_j}\}} \frac{\Delta y_T}{S_T^2} \left[\left(\sum_{i \in i_T} x_i \Delta \psi_i \right)^2 + \left(\sum_{i \in i_T} y_i \Delta \phi_i \right)^2 + \left(\sum_{i \in i_T} y_i \Delta \psi_i \right)^2 + \left(\sum_{i \in i_T} x_i \Delta \phi_i \right)^2 \right] \\ \frac{\partial \mathcal{F}_a}{\partial y_j} &= \left(\frac{1}{4} \sum_{T \in \{T_{h_j}\}} J_T \frac{\vec{l}_T \cdot \vec{l}_T}{S_T} \right) y_j + \frac{1}{4} \sum_{i \in i_j} \left(J_T \frac{\vec{l}_{i-1} \cdot \vec{l}_T}{S_T} + J_{T+1} \frac{\vec{l}_{i+1} \cdot \vec{l}_{T+1}}{S_{T+1}} \right) y_i \quad (41) \\ &\quad + \frac{1}{16} \sum_{T \in \{T_{p_j}\}} \frac{\Delta x_T}{S_T^2} \left[\left(\sum_{i \in i_T} x_i \Delta \psi_i \right)^2 + \left(\sum_{i \in i_T} y_i \Delta \phi_i \right)^2 + \left(\sum_{i \in i_T} y_i \Delta \psi_i \right)^2 + \left(\sum_{i \in i_T} x_i \Delta \phi_i \right)^2 \right] \end{aligned}$$

where additional algebra is required to get the above two equations although it is the direct results of differentiation of equaiton (27). The most significant difference is the third terms in equations (40) and (41). A close look at these terms for one cell shows that these terms in pair try to enlarge a cell area by moving a node j in the direction perpendicular to the opposite side. Here is the mechanism against mesh tangling(This point of view has been pointed out in [1]). On the other hand, the first two terms in (40) and (41) are the standard FEM with Jacobians as weights. The changes to x_j and y_j are thus biased toward the elements with large Jacobians. This is the form of mesh adaptation for the asymmetric norm. The comparisons of the two norms are summarized in Table.1. From these theoretical comparisons, we may be tempted to conclude that the symmetric norm is the better choice because the problems are linear. But we still extend the comparison to numerical experiments.

5 Implementation

Duplicating a method of steepest descent, we write a scheme as

$$\mathbf{U}_j^{n+1} = \mathbf{U}_j^n - c \frac{\partial \mathcal{F}}{\partial \mathbf{U}_j} \quad . \quad (42)$$

The symmetric norm	The asymmetric norm
• Always positive	• Can be negative for negative $S_{T_{(x,y)}}$'s.
• No decoupling	• Decoupling of (ϕ, ψ), and (x, y)
• Linear problem for (ϕ, ψ)	• Linear problem for (ϕ, ψ)
• Linear problem for (x, y)	• Nonlinear problem for (x, y)
• Mesh adaptation in (ϕ, ψ) plane driven by large $S_{T_{(x,y)}}$'s, with the mechanism against small areas.	• Standard FEM for (ϕ, ψ)
• Mesh adaptation in (x, y) plane driven by large $S_{T_{(\phi,\psi)}}$'s, with the mechanism against small areas.	• Mesh adaptation in (x, y) plane driven by large Jacobians, with the mechanism against small areas.

Table 1: The comparison of the symmetric norm and the asymmetric norm.

As mentioned earlier, we update (ϕ, ψ) and (x, y) alternately so that the problem is divided into two linear problems (the symmetric norm). The steepest descent method is, however, well-known to be very slow because of its dimensional inconsistency.

Consider two procedures; update all the quantities in the domain at one time or update the quantities successively. The former is a Jacobi type iteration (steepest descent) while the latter is a Gauss-Seidel type one. Naturally the latter is expected to be faster than the former. And it has been demonstrated in [6]. However one finds it still very slow in practice. Also one must find the constant factor c which gives faster convergence from a number of trial computations. However as touched on in the previous section, for the Cauchy-Riemann equations we have one way to figure out how big or small the constant should be. We return to the equations (34) to (41). And we immediately see that the scheme can be dimensionally consistent if the gradients are multiplied by the coefficient of the solution or coodinate values at j,

$$\left(\frac{1}{4}\sum_{T\in T_j}\vec{l}_T\cdot\vec{l}_T\right) \quad or \quad \left(\frac{1}{4}\sum_{T\in T_j}\frac{\vec{l}_T\cdot\vec{l}_T}{S_T}\right) \quad . \tag{43}$$

Thus the update formula becomes, for instance,

$$\phi_j^{n+1} = \phi_j^n - \omega\left(\frac{1}{4}\sum_{T\in T_{p_j}}\vec{l}_T\cdot\vec{l}_T\right)^{-1}\frac{\partial\mathcal{F}}{\partial\phi_j} \quad . \tag{44}$$

Specially for equations (36) and (37) the scheme is indistinguishable from SOR. And we already know that the best value of ω lies between 1.0 and 2.0, and approaches 2.0 as the size of the problem increases, although this requires us to find the best value from a number of experiments. However in this way, convergence characteristics has been surprisingly improved. Not only are the convergence for equations (36) and (37) improved, but also those of other gradients can be improved in the same way. Nevertheless equations (40) and (41) still have poorer convergence characteristics due to their nonlinearity. For the present we treat the Jacobians in the expression as constants and follow the procedure explained above.

6 Numerical experiments

6.1 Test problem

Numerical experiments were performed for a two dimensional flow consisting of a square box with a source in one corner and a sink in the other. The flow is actually similar to the well-known lid-driven cavity flow. The difference lies in the fact that the no-slip condition at the wall cannot apply in such a potential flow. Thus all the boundaries are streamlines in this case. And also the velocity along the upper wall is not constant. There exists the

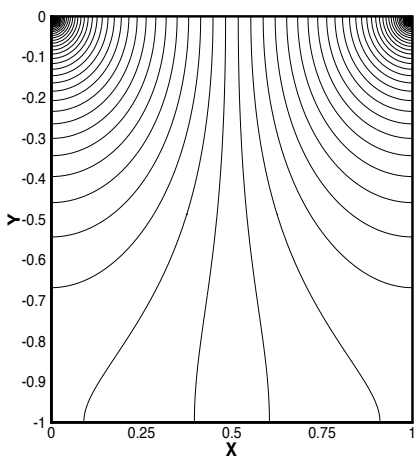

Figure 3: Contour plot of the exact solution of ϕ. 70 Levels, k=22

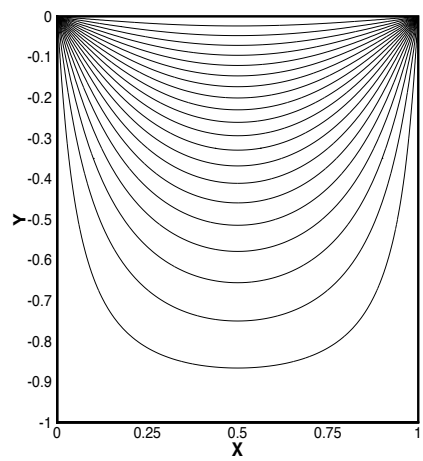

Figure 4: Contour plot of the exact solution of ψ. 20 Levels, k=22

exact solution for this problem which is expressed in terms of the complex potential $F(z)$,

$$F(z) = \phi + i\psi = m \ln \left[sinh \frac{\pi z}{2a} \frac{\prod_{k=even} \left(1 - sinh^2 \frac{\pi z}{2} / sinh^2 \frac{k\pi}{2a}\right)}{\prod_{k=odd} \left(1 - sinh^2 \frac{\pi z}{2} / sinh^2 \frac{k\pi}{2a}\right)} \right] \tag{45}$$

where $z = x + iy$ and m determines the source(and sink) strength. In fact, this solution produces a series of square regions which are divided by streamlines, depending on the value of k. The solution can be shown to converge quite rapidly, so that $k = 22$ which we used is more than enough. We choose the domain of interest Ω as the unit square whose upper left corner coincides with the origin, i.e. $\Omega = \{(x, y) | 0 \leq x \leq 1, -1 \leq y \leq 0\}$. The source strength was chosen to be $-\frac{2}{\pi}$ and a was set to be 1 such that the stream function takes the value of zero when $y = 0$ and the value of unity elsewhere on the boundary. These were used as the boundary conditions for our numerical experiments. And also the quantity inside the square bracket was divided by itself with $z = \frac{a}{2}$ inserted, so that it becomes unity at $x = \frac{a}{2}$, i.e. the potential becomes zero at the mid point of the upper boundary. As for ϕ however we do not specify any value on the boundary in our computations since changing ϕ by a constant has no significance as mentioned earlier. Therefore we update ϕ on the boundary. The exact solutions in Ω are shown in Figure(3)

and (4). The most difficult part of this problem is the singularities at two upper corners. It is indeed not obvious what values we should assign there as the boundary conditions. For this reason, we updated both of the solutions at these points. For the initial values for ϕ and ψ, we always used the values of zero for both.

6.2 Convergence criteria

Convergence criteria must be determined by fair means for each morm. In our experiment, we compute a L1 norm for all the changes divided by the relaxation factors, $\frac{\delta\phi}{\omega}$ for instance, and stop the calculation when it reaches below a tolerance. The tolerance was always set to be 10^{-5}. This seems to be a fair way since we use the same value of ω, although we must use much smaller values for δx_j and δy_j of the asymmetric norm. In the actual computaitons, we used $\omega = 1.7$ for all the updates except for the nonlinear case where $\omega = 0.05$ was used. In fact, the tolerance may depend on the mesh size especially for the standard method. In such a case, the L1norm is closely related to the truncation error of the discretization for a structured grid. However it does not apply once the grid starts to deform. We treat the problem as a minimization. Then it is reasonable to stop the minimization when the gradients are small.

6.3 The Results

When working with the symmetric norm there is no guarantee that the element areas will remain positive, and instead we find experimentally that if initial grid of solutions (ϕ, ψ) is degenerate, the method actually converges to a tangled mesh, as shown in Figure 7. The method converged at 3158 iterations, and during which there was no way to notice that the mesh had been tangled. The corresponding solutions are plotted in Figures 8 and 9. It is a little surprise that the solutions are not spoiled so destructively. The cause of the tangling lies in the fact that one iteration for ϕ and ψ is not enough to make an initial triangulation in the hodograph plane. Mesh movement should be activated when fairly good solutions are obtained, i.e. some kind of initial triangulation in ϕ-ψ plane. In the next calculation, we then fixed the grid for the first 30 iterations in order to see whether the mesh tangling occurs again. As shown in Figure 10, the mesh tangling never occured in this case.

Shown in Figure 11 is the result for the asymmetric norm. This grid was obtained by updating x and y from the beginning of the iteration. We see from the figure that no tangling occured. The convergence is extremely slow for the asymmetric case as we expected. In fact the solutions blow up for any value exceeding 0.05. In both symmetric and asymmetric cases, it can be seen in the figures that the nodes moved toward the two upper corners where the solutions change rapidly. It is also observed that the converged grid is more symmetric for the asymmetric norm than that for the symmetric norm.

The results of the numerical experiments are summarized in Table.2 and 3. Please note that we do not include the values of ψ at the two upper corners in computing the errors. From these tables, we notice that the solutions are in fact not improved by the grid movements. The errors increase rather than decrease when we allow the grid to move. This implies that minimizing the residuals does not imply minimizing the local error.

Clearly the convergence is faster for the symmetric norm. As mentioned earlier, this may be due to the fact that the asymmetric norm yields the nonlinear problem for x and

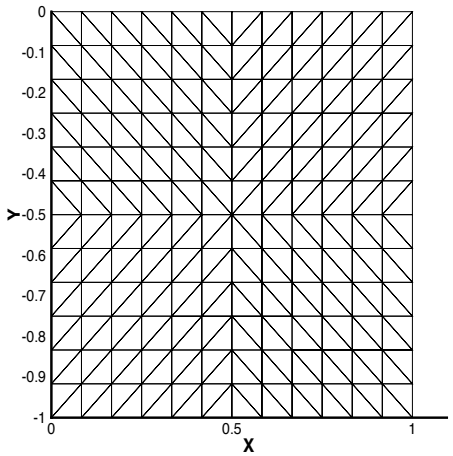

Figure 5: The initial grid

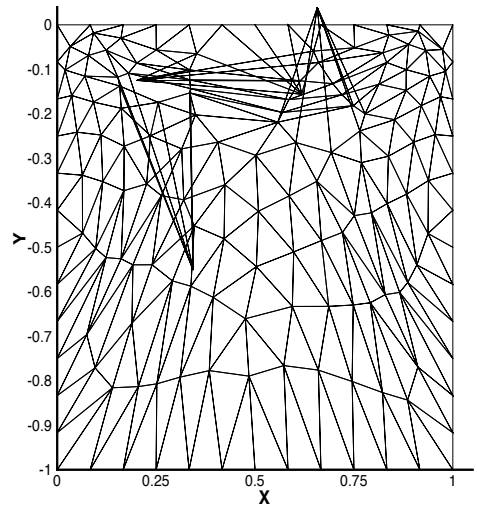

Figure 6: The converged grid for the symmetric norm, 3158 iterations

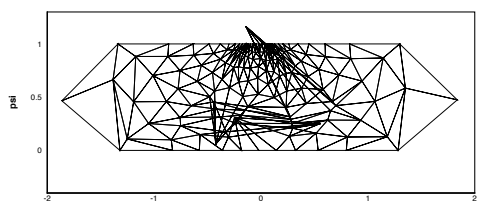

Figure 7: The converged grid in ϕ-ψ plane for the symmetric norm, 3158 iterations

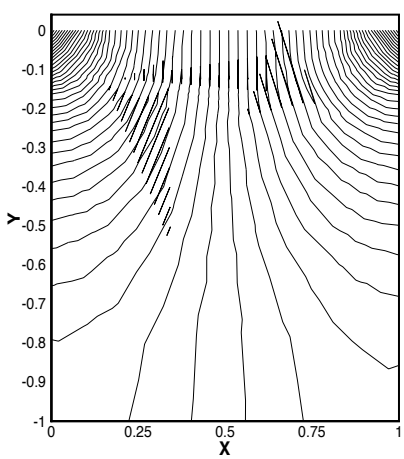

Figure 8: Contour plot of ϕ for the symmetric norm, 70 Levels, 3158 iterations

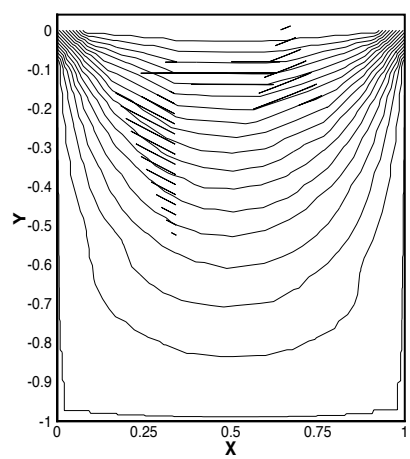

Figure 9: Contour plot of ψ for the symmetric norm, 20 Levels, 3158 iterations

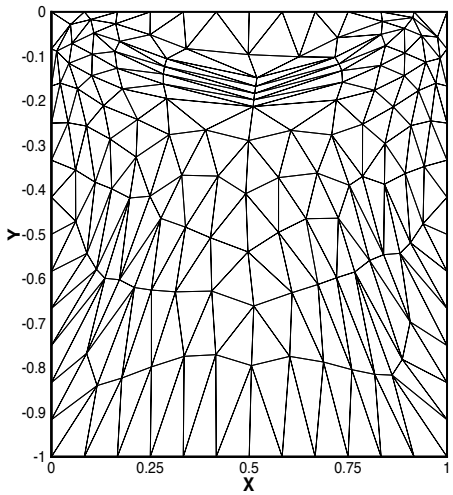

Figure 10: The converged grid for the symmetric norm, 2044 iterations

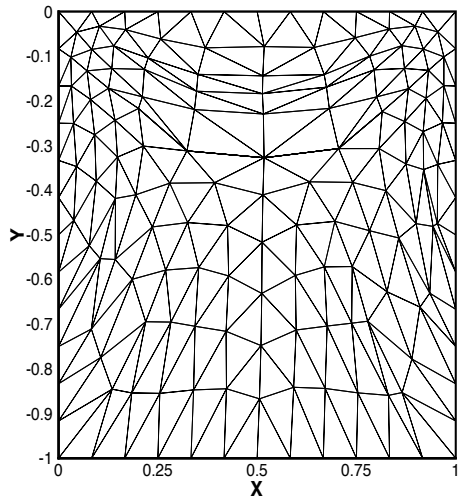

Figure 11: The converged grid for the asymmetric norm, 1735 iterations

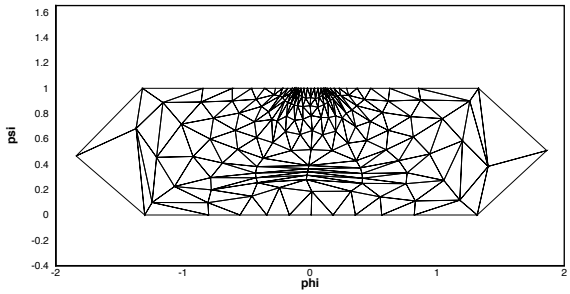

Figure 12: The converged grid in ϕ-ψ plane for the symmetric norm, 2044 iterations

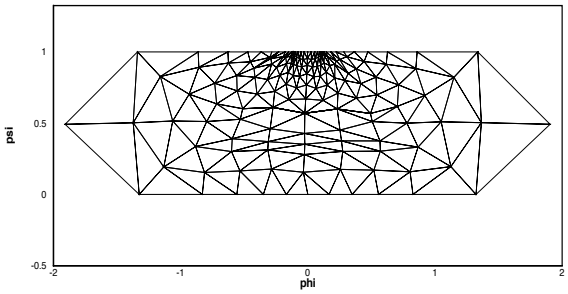

Figure 13: The converged grid in ϕ-ψ plane for the asymmetric norm, 1735 iterations

	Fixed grid	Moving grid	Moving grid after 30 iterations
Iteration number	35	3158	2044
Norm	6.30875E-04	1.66999E-04	1.48090E-04
L1(U_T)	6.45785E-04	6.24807E-04	6.20536E-04
L1(V_T)	6.63585E-04	6.00813E-04	5.79348E-04
L1(error in ψ)	1.18004E-03	1.18007E-02	5.65812E-03

Table 2: The results of the numerical experiments for the symmetric norm

	Fixed grid	Moving grid
Iteration number	35	1735
Norm	1.81692E-01	9.73940E-02
L1(U_T)	6.45785E-04	6.02370E-04
L1(V_T)	6.63586E-04	5.79919E-04
L1(error in ψ)	1.18004E-03	2.19666E-03

Table 3: The results of the numerical experiments for the asymmetric norm

y. Yet there is another reason for this. For the asymmetric norm the decoupling of ϕ and ψ occurs. Then the two variables are related to each other only on the boundary in the form of the discrete versions of the Cauchy-Riemann equations. This happens to play a role as the boundary condition for ϕ. Hence all the interior values of ϕ receive the information from the boundary, which takes some time to spread over the domain. On the other hand, the update formulae for ϕ and ψ in the case of the symmetric norm involve both variables on unstructured grid (on structured grid, the two norms yields the same scheme for ϕ and ψ). It can be shown that the scheme is not the discretized versions of Laplace equations but those of the Cauchy-Riemann equations. Therefore ϕ receives the information concerning with the boundary condition immediately at every node in the domain. This appears to accelerate the convegence. In order to see this fact, we ran the codes on an unstructured grid without grid movement. It was observed that the symmetric norm version converges more than twice as fast as the asymmetric version, i.e. the standard finite element method.

7 Concluding Remarks

Two different norms of a discrete least square method for Cauchy-Riemann equations were studied. The mechanisms by which each norm produces the solutions and the grid was revealed. It was shown that both schemes produced the approximate solutions and the grids, but with error increased. Also it was found that the method converged on a tangled mesh in the symmetric norm case. At this time, it would be premature to judge which is the better choice because the error increases in both cases. Thus our attempt to improve the solution by grid movement failed. In order to achieve the goal, a theoretical study about the error is necessary, or even a different formulation may be of value such as minimizing two different types of norms,i.e. one for the solution and the other for the grid. Also further convergence acceleration and the study about the singularity are included in the future work.

References

[1] P. L. Roe, Compounded of many simples reflections on the role of model problems in CFD, August 1996.

[2] C. Johnson, Numerical solution of partial differential equations by the finite element method, Cambridge university press, Cambridge, 1987.

[3] P. G. Ciarlet , Introduction to numerical linear algebra and optimisation, Cambridge university press, Cambridge, 1989.

[4] A. Borzi, K. W. Morton, E.Suli, and M. Vanmaele, Multilevel Solution of Cell Vertex Cauchy-Riemann Equations. SIAM J. Sci. Comput. Vol.18 No.2 pp.444-459, March 1997.

[5] M. J. Baines, Algorithms for Optimal Discontinuous Piecewise Linear and Constant L_2 Fits to Continuous Functions with Adjustable Nodes in One and Two Dimensions. Mathematics of Computation. Vol.62 No.206 pp.645-669 April 1994.

[6] M. Y. Tourigny and F. Hulsemann, A New Moving Mesh Algorithm for The Finite Element Solution of Variational Problems.

[7] P. M. Gresho and R. L. Sani, On Pressure Boundary Conditions for the Incompressible Navier-Stokes Equations. Finite Element in Fluids, vol.7 , 1987.